

## Rheology of nanocrystal-bearing andesite magma and its roles in explosive volcanism

Satoshi Okumura<sup>1✉</sup>, Kentaro Uesugi<sup>2</sup>, Akio Goto<sup>3</sup>, Tatsuya Sakamaki<sup>1</sup>, Kazuhisa Matsumoto<sup>1</sup>, Akihisa Takeuchi<sup>2</sup> & Akira Miyake<sup>4</sup>

Recent petrological and experimental studies have proposed that explosive volcanism may originate from the formation of nanoscale crystals in magma and the resultant ductile-brittle transition. However, the rheology of magma with quantified volume fractions of nanoscale crystals has not been investigated before, and thus, the formation of nanoscale crystals causing magma fragmentation that explains the origin of explosive eruptions is not conclusive. Here, we investigate the rheology of andesite magma with nanoscale crystals (magnetite). For this, a glass fibre elongation experimental apparatus with a heating furnace was developed at the synchrotron radiation X-ray system (SPring-8). During melt elongation, we observed the formation of crystals using small-angle X-ray scattering and wide-angle X-ray diffraction. Our experimental data demonstrate that magma viscosity increases with the formation of nanoscale crystals, but the degree of the increase is much lower than that predicted from analogue materials. Finally, we conclude that nanocrystal formation in intermediate composition magmas cannot explain rheological transition and other mechanisms such as nanocrystal agglomeration (not observed in our experiments) and/or heterogeneous nucleation of gas bubbles on nanocrystals are required to induce mafic to intermediate explosive volcanisms.

<sup>1</sup>Division of Earth and Planetary Materials Science, Department of Earth Science, Graduate School of Science, Tohoku University, Sendai 980-8578, Japan.

<sup>2</sup>SPring-8/Japan Synchrotron Radiation Research Institute, Sayo, Hyogo 679-5198, Japan. <sup>3</sup>Center for Northeast Asian Studies, Tohoku University, Sendai, Miyagi 980-8576, Japan. <sup>4</sup>Division of Earth and Planetary Sciences, Graduate School of Science, Kyoto University, Kitashirakawa Oiwake-cho, Sakyo-ku, Kyoto 606-8502, Japan.

✉email: [satoshi.okumura.d2@tohoku.ac.jp](mailto:satoshi.okumura.d2@tohoku.ac.jp)

**B**rittle magma fragmentation is a key process for explosive volcanism. The fragmentation results in a flow-type transition in a volcanic conduit from bubbly magma flow to gas-particle flow, leading to the explosive release of magma fragments and volcanic gases to the surface<sup>1,2</sup>. Brittle magma fragmentation occurs when the timescale of magma deformation is shorter than that of structural relaxation<sup>3</sup>. Structural relaxation depends on magma chemistry; silicic magmas have longer relaxation timescales than relatively mafic and depolymerised magmas. For silicic magmas, it has been confirmed that the deformation rate of magma during its ascent to the surface is sufficiently high to cause brittle magma fragmentation<sup>4–7</sup>. However, low-viscosity magmas such as basaltic and andesitic magmas, which have short relaxation timescales, do not undergo brittle fragmentation easily, although such magmas have also been known to cause explosive eruption<sup>8,9</sup>.

This problem can be partially resolved by considering the effect of crystals on magma rheology. Magma viscosity increases by several orders of magnitude when the crystal volume fraction reaches the critical value, which is ~30 vol% for anisotropic crystals, such as plagioclase microlites<sup>10</sup>, and ~50 vol% for isotropic crystals<sup>11</sup>. During magma ascent and decompression, crystals, in particular plagioclase, form because of the change in the liquidus, which is strongly affected by water content in magma<sup>12,13</sup>. Therefore, brittle fragmentation can occur if the crystal contents reach critical values through decompression-induced crystallisation during magma ascent to the surface<sup>9</sup>. A recent experimental study<sup>14</sup> proposed that magma viscosity increases by one to two orders of magnitude even at low crystal content, i.e., a few volume percentages, when nanoscale crystals are formed, based on viscosity measurements of mixtures of silicon oil and spherical SiO<sub>2</sub> nanoparticles. If their results are applicable to nanocrystal-bearing magmas, magma fragmentation may occur more easily than initially thought, because nanoscale crystals are often observed in natural intermediate to mafic magmas<sup>14–18</sup>. However, rheological studies on fluids with nanoparticles (nanofluids) demonstrate the complex effects of nanoparticles on viscosity<sup>19</sup>. For instance, particle size and surface area, pH of fluid, and the charge at the particle

surface influence the agglomeration of nanoparticles in a nanofluid and markedly impact the nanofluid viscosity. Therefore, the effect of nanocrystals on magma viscosity needs to be investigated for actual magmas.

An experimental difficulty to determine the crystal-free melt viscosity is a problem for investigating the effect of nanocrystals on magma viscosity. Since nanocrystals can form during high-temperature experiments<sup>20,21</sup>, they must be identified directly during the experiments. A careful evaluation of the effect of nanocrystals on magma viscosity based on viscosity measurements combined with calorimetry, Raman spectroscopy, and transmission electron microscopy confirmed that the presence of nanocrystals in magma produces an increase in magma viscosity<sup>21</sup>; however, no previous study has successfully measured the viscosity of magma with a known amount of nanocrystals.

To clarify the effect of nanoscale crystals on magma rheology quantitatively, we measure the viscosity of an andesitic magma with a quantified volume fraction of nanoscale crystals for the first time. For this, we combine an originally developed deformation apparatus<sup>22</sup> with a small-angle X-ray scattering (SAXS) and wide-angle X-ray diffraction (WAXD) system and directly measure the size and volume fraction of crystals during viscosity measurements. The details of the experimental system are summarised in Supplementary Information and Supplementary Fig. 1.

## Results

### Heat and quench experiments: calibration of crystal size and volume fraction.

We first performed heat and quench experiments using the same furnace as in situ experiments to calibrate the crystal size and volume fraction estimated by SAXS. The samples used were andesite glass fibres prepared from a volcanic bomb collected at the Sakurajima volcano (see the “Methods” section). The chemical composition of the glass fibre is listed in Supplementary Table 1 and Supplementary Data 1. In the prepared glass fibres, no nanocrystals were observed, based on transmission electron microscopy (TEM) at Kyoto University (Fig. 1a) and WAXD (Supplementary Fig. 2) at BL47XU of SPring-8 (Japan).

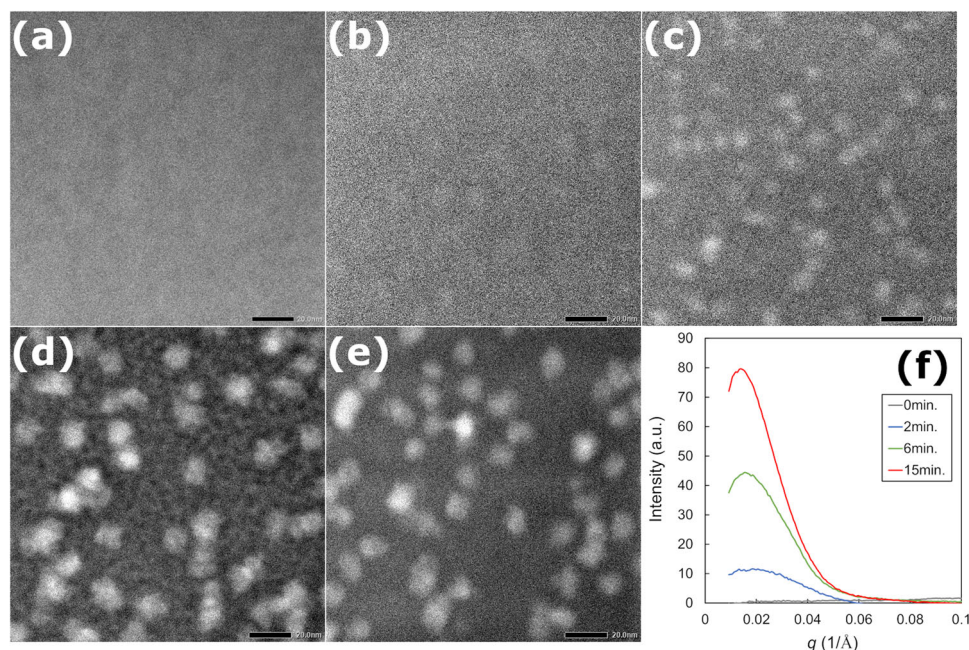


**Fig. 1** ADF-STEM images and SAXS of quenched samples. **a** ADF-STEM images obtained for a glass fibre without any heating after preparation. No crystals were observed. **b–e** ADF-STEM images were obtained for samples after dwell times of 0, 2, 6, and 15 min and rapid cooling. Scale bars represent 20 nm. **f** SAXS obtained for samples in (**b–e**).

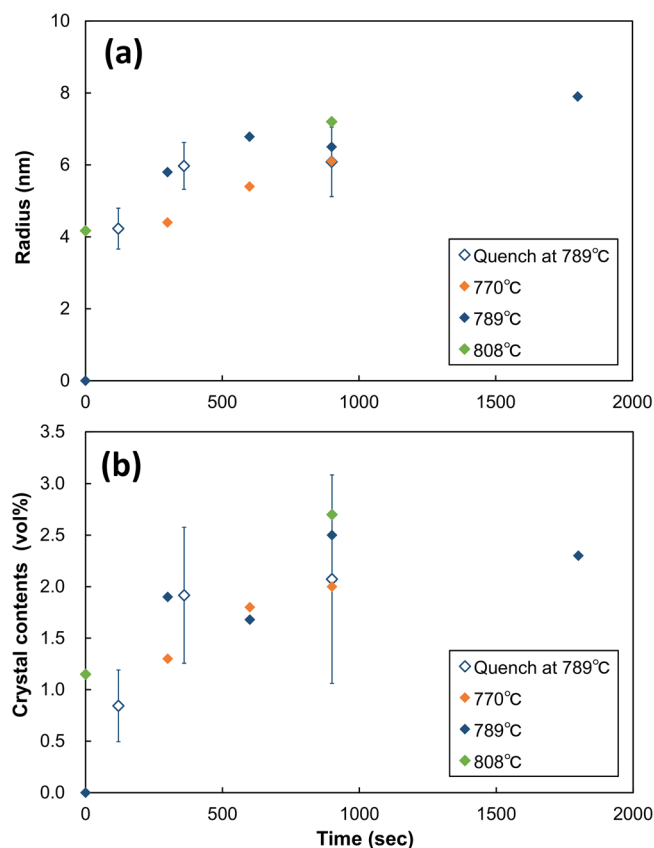


**Fig. 2 Time evolution of radius and volume fraction of crystals.** In **a**, **b**, the radius and volume fraction obtained at 770, 789, and 808 °C are shown, respectively. The data expressed by open symbols are from TEM analyses for quenched samples, while solid symbols are from SAXS analyses. The error bars represent the standard deviation. The data are summarised in Supplementary Table 2.

In this experiment, the samples were heated to 789 °C at a rate of 23 °C per minute and then maintained at this temperature for 0, 2, 6, and 15 min. The recovered samples were measured by SAXS at BL47XU of SPring-8 and TEM at Kyoto University (Fig. 1). As demonstrated both in SAXS and TEM (annular dark-field scanning TEM, ADF-STEM) images, nanoscale crystals formed during heating and their size and volume fraction increased with time (Fig. 2). In the samples with a heating dwell time of 0 min, no clear crystals were observed, corresponding to no SAXS signal (Fig. 1b, f). Here, we noted that the melt structure continued to change during heating to the experimental temperature, which may have formed a pre-crystal structure in the melt, although no clear crystals were observed by the TEM, SAXS, and WAXD analyses. To determine the size and volume fraction of nanocrystals using SAXS in the following in situ experiments, we first determined their size in quenched samples with dwell times of 2, 6, and 15 min based on the ADF-STEM images. The size could also be determined from SAXS, assuming spherical crystals for the same samples. The size differences obtained by the two different methods agree within the relative errors of 30% (Supplementary Fig. 3). Subsequently, the crystal volume fractions were estimated from the number and radius of crystals in the ADF-STEM images by assuming a spherical crystal and 100 nm of thickness for the TEM thin section, confirmed under a focused ion beam scanning electron microscope (see Supplementary Information). Finally, the volume fractions of crystals obtained from SAXS were calibrated against those estimated above (Supplementary Fig. 3). Based on this calibration,

we determined the size and volume fraction of nanoscale crystals in situ during viscosity measurements using SAXS.

The nanocrystal phase was determined based on WAXD, obtained using two-dimensional flat panels simultaneously with SAXS measurement at SPring-8 (Supplementary Fig. 2a). From the WAXD data, the nanocrystals were determined to be magnetite. We could not determine the phase for each grain under TEM, because the diffraction pattern was too weak. A compositional map of a quenched sample under TEM indicates that nanocrystals are iron oxides and that no clear spatial variation of major elements in the melt was yielded by the formation of nanocrystals (Fig. 3). However, additional observations with higher spatial resolution will be required to clarify the chemical heterogeneity around the nanocrystals, as discussed in the following section.

**In situ rheological measurement of nanocrystal-bearing andesite magma.** We performed fibre elongation experiments at temperatures of 731, 750, 770, 789, 808, and 828 °C at BL47XU of SPring-8 (see the “Methods” section, Supplementary Table 2 and Supplementary Data 1). In these experiments, the samples were first heated to the experimental temperature at rates of 20–23 °C per minute and then held at that temperature for 0, 5, 10, 15, and 30 min. After the dwell time of 0–30 min, the samples were elongated for 200 s at a rate of 100  $\mu\text{m s}^{-1}$ . For these experiments, the sample length was 24–30 mm, resulting in strain rates of 0.003–0.004  $\text{s}^{-1}$ . During the heating and elongation experiments, SAXS measurements were repeated every 100 ms (see Supplementary Information and Supplementary Fig. 4). All run information is summarised in Supplementary Table 2 and Supplementary Data 1.

In our experiments, both viscous elongation and brittle failure of the samples were observed (Fig. 4). When the samples were viscously elongated, the load for sample deformation increased and then decreased gradually, although the load rapidly decreased in the case of brittle failure (see Supplementary Fig. 5). The brittle failure was observed at relatively low temperatures and long heating times (Fig. 4). For instance, only viscous elongation was observed at 808 °C, although brittle failure occurred at 731 °C. At 789 °C, the sample was viscously elongated at the dwell time of 0 min, but brittle failure was observed when the sample was elongated after heating for >15 min.

The size and volume fraction of nanoscale crystals determined based on the SAXS measurement increased with an increase in dwell time at experimental temperatures, as observed in the quench experiments (Fig. 2, Supplementary Table 2 and Supplementary Data 1). The increase rates in the size and volume fraction of crystals are higher at higher experimental temperatures. During the heating to experimental temperatures, the crystallisation can start; at experimental temperatures >808 °C, nanocrystals already formed when the temperature reached the desired ones. At <789 °C, the nanocrystals were not detected when the dwell time at experimental temperature was 0 min, based on the SAXS analyses (Supplementary Fig. 4). The WAXD also observed that no crystals formed at <789 °C when the dwell time was 0 min, while a small peak was observed at 808 °C (Supplementary Fig. 2b). These results indicate that at <789 °C, nanocrystals did not form during the heating up to the experimental temperature, and the viscosity obtained at the dwell time of 0 min represents nanocrystal-free melt viscosity.

We calculated magma viscosity based on the observed load during viscous elongation (see Supplementary Information). When we compare nanocrystal-free melt viscosities measured in this study with those calculated at the same condition, using the previous model<sup>23</sup> for the chemical composition of the glass fibre listed in Supplementary Table 1 and Supplementary Data 1, our



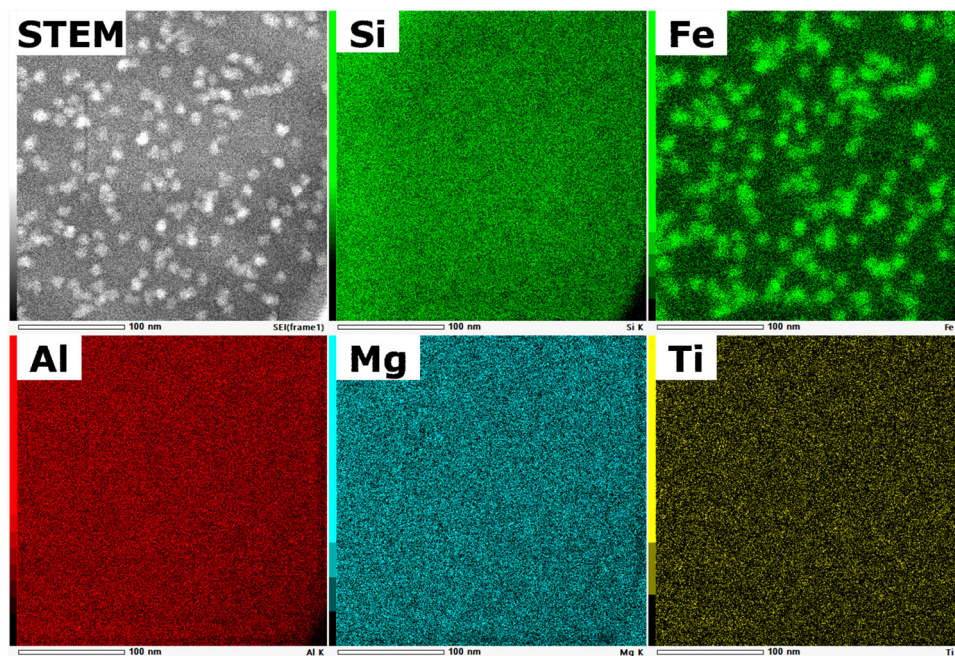


**Fig. 3** A STEM image and EDX composition map (Si, Fe, Al, Mg, and Ti) of a quenched sample (15 min heating). Scale bars represent 100 nm.

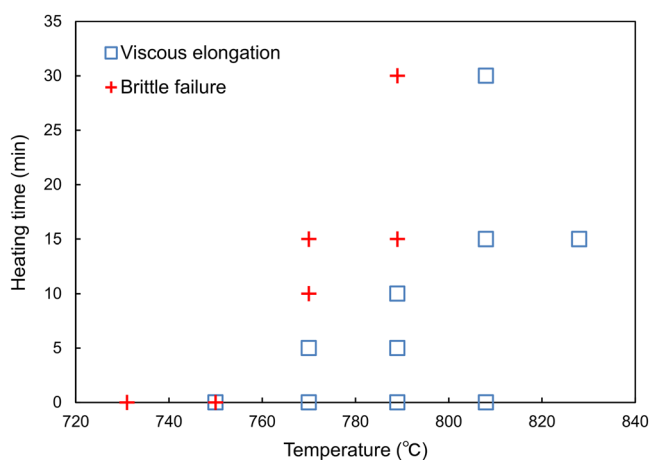


**Fig. 4** Deformation type, i.e., viscous elongation and brittle failure, of andesite melts under a strain rate of 0.003–0.004 s<sup>-1</sup>. Brittle failure is observed at low temperatures and long heating duration. The data are summarised in Supplementary Table 2.

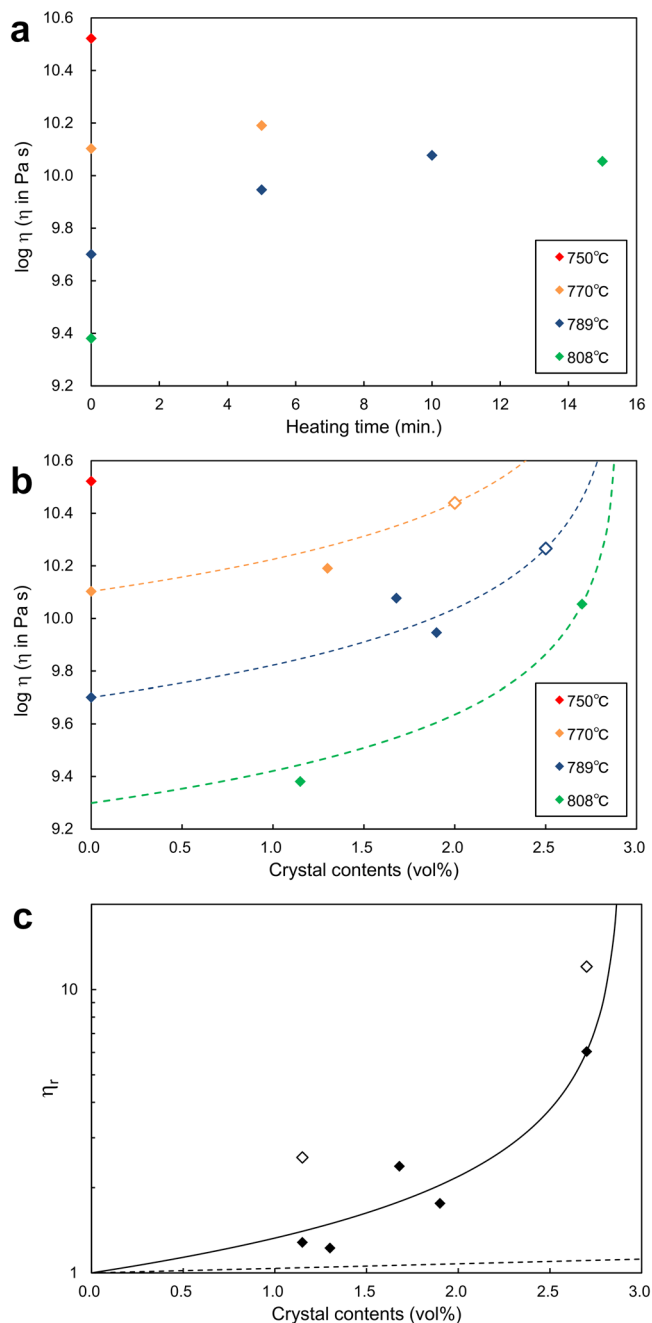
data are systematically higher than the calculated values, but both viscosities are consistent within 0.3 in log unit (Supplementary Information, Supplementary Table 2 and Supplementary Data 1). This small discrepancy can originate from the temperature distribution in the furnace and the resultant localisation of the deformation, although recovered samples did not show strong localisation<sup>22</sup>. Additionally, the melt structure can continue to change during heating to the experimental temperature, which may have formed a pre-crystal structure in the melt and caused an increase in melt viscosity, although no detectable nanocrystals formed in the sample heated at <789 °C with the dwell time of 0 min. The model calculation also includes uncertainties; in particular, the previous model<sup>23</sup> does not consider the effect of ferric-ferrous iron, which influences the viscosity<sup>24</sup>.

Figure 5a, b demonstrate the relationship between heating duration and magma viscosity, and the volume fraction of crystals and magma viscosity, respectively. The effect of nanocrystal formation on magma viscosity is clarified in Fig. 5c, in which

magma viscosity was normalised by the viscosity of the nanocrystal-free melt. Here, we used melt viscosity calculated based on the previous model<sup>23</sup> when the viscosity was not measured because of the rapid formation of nanocrystals at a relatively high temperature (808 °C), and the calculated melt viscosity was modified by adding the viscosity in 0.3 log units, based on the comparison between the measured and calculated viscosities described above. The viscosity increases with time, and it seems to approach a constant value (Fig. 5a). The viscosity is almost the same when samples were heated for 15 and 30 min at 808 °C before the elongation (Supplementary Table 2 and Supplementary Data 1). This is because nanocrystals grew with time and the volume fraction of the nanocrystals approached a constant value (Fig. 2). Furthermore, the magma viscosities increased with the volume fraction of crystals (Fig. 5b, c). Under constant melt viscosity, the effect of micro/macro-particles in a fluid on bulk viscosity has been described by the Krieger–Dougherty equation<sup>25</sup>, i.e.,  $\eta_r = (1 - \phi/\phi_m)^{-B\phi_m}$ , where  $\phi$  is the crystal content,  $\phi_m$  is the maximum packing fraction, and  $B$  is the Einstein coefficient. Here, we applied this model to our experimental data; however, it should be noted that the experimental data in Fig. 5c reflects the effect of changes in melt composition in addition to the effect of the formation of solid particles, as discussed in the following section.

## Discussion

**Effect of nanocrystal formation on magma viscosity.** Our experimental data indicate that nanocrystal formation in magmas increases the magma bulk viscosity. At least two processes influence this result: changes in melt composition induced by crystallisation and the formation of solid particles. First, crystallisation in magmas changes the composition of the melt; therefore, melt viscosity can change with crystallisation. In the case of magnetite crystallisation, the change in the ferric–ferrous ratio and increase in silica content in melt influence the viscosity<sup>26</sup>. The ferric and ferrous irons are the network-former and network modifier cations<sup>20</sup>; when the network-forming Fe<sup>3+</sup> is relatively extracted compared with the network-modifying Fe<sup>2+</sup>, melt viscosity can decrease rather than increase<sup>20,24</sup>. It should be noted



**Fig. 5 Viscosities of andesitic melt with nanocrystals.** **a** Viscosity as a function of heating time before deformation. **b** Relationship between viscosity and crystal content. The errors in the viscosities obtained from the load, sample size, and elongation rate are much smaller than 0.1 in log units. The viscosity increases with crystal content and the viscosity is higher at lower temperatures. Dashed curves represent viscosities at each temperature (770, 789, and 808 °C) predicted by the equation obtained in **(c)**. Open oranges and blue diamonds represent the predicted viscosities at 1.8 and 2.5 vol% crystals, respectively, which correspond to those just before brittle failure after 10 and 15 min heating. **c** Relationship between relative viscosities (i.e., magma viscosity normalised by crystal-free melt viscosity) and crystal content. Crystal-free melt viscosity at 808 °C was calculated using the previous model<sup>23</sup> and modified based on a comparison between our data and the model calculations (see text). Open symbols represent values calculated using the original melt viscosity without any modification. The solid curve is a fitting curve on experimental data, expressed as  $\eta_r = (1 - \phi/0.029)^{-0.67}$ , where  $\phi$  is the volume fraction of crystals. A dashed curve indicates viscosities predicted from the previous model<sup>29</sup> with an assumption of a crystal aspect ratio of 1.

chemically differentiated layer around nanocrystals may increase the effective volume of the solid particles and contribute to increasing the viscosity<sup>21</sup>; however, we could not observe any chemical heterogeneity around the nanocrystals, although additional observations using a higher spatial resolution are required to confirm this effect (Fig. 3). Therefore, the increase in magma viscosity with crystallisation seems to be mainly attributed to the increase in melt viscosity caused by the changes in the melt composition.

In nanofluids, it has been shown that nanoparticle agglomeration strongly enhances viscosity<sup>14,30</sup>, although the agglomeration of nanocrystals was not observed under elongation in this study. In nature, magma flow in a volcanic conduit experiences shear flow<sup>5,31,32</sup> and hence may result in collision and agglomeration of nanocrystals. Indeed, the agglomeration of nanocrystals was found in low-viscosity basaltic magmas<sup>14</sup>, while they do not show agglomeration in intermediate-composition magmas<sup>15</sup>. Additional experimental investigations under shear flow are needed to confirm whether nanocrystals agglomerate in actual magmas and whether this results in an increase in magma viscosity.

**Brittle failure of nanocrystal-bearing magma.** Our experiments demonstrated that nanocrystal formation enhances the brittle failure of magma. For instance, brittle failure was observed when the samples were held for 10 and 15 min at 770 and 789 °C, respectively, although the samples showed only viscous elongation under shorter dwell times at high temperatures. This enhancement of brittle failure can be explained by considering the increase in magma viscosity.

In Fig. 5b, the viscosity change with crystal content is predicted at each experimental temperature based on the Krieger–Dougherty equation<sup>25</sup>. Using this prediction and the crystal contents, we can estimate the viscosities of magmas in experimental runs with brittle failure at 770 and 789 °C. For the runs, i.e., the heating for 10 and 15 min at 770 and 789 °C, the crystal contents were estimated to be 1.8 and 2.5 vol%, respectively (Fig. 2); thus, the magma viscosities obtained were  $2.4 \times 10^{10}$  and  $1.8 \times 10^{10}$  Pa s at 770 and 789 °C (Fig. 5b). In our experiments, the strain rate was  $0.003\text{--}0.004\text{ s}^{-1}$ ; hence, the products of viscosity and strain rate are calculated to be  $0.83 \times 10^8$  and  $0.66 \times 10^8$  Pa at 770 and 789 °C, respectively. These values are consistent with the criterion for the brittle failure of magma not including nanocrystals ( $\sim 10^8$  Pa)<sup>4,7</sup>. This result indicates that nanocrystal formation causes the increase in magma viscosity,

that the redox condition in the melt did not change during the viscosity measurements via the oxidation of the outer sample, because only a few micrometres of the sample are influenced by the oxidation when the oxidation rate is limited by diffusion<sup>27,28</sup>. On the other hand, the depletion of iron content results in a relative increase in silica content, causing an increase in melt viscosity. When we estimate the change in melt viscosity based on the previous model<sup>23</sup>, the complete depletion of iron in the melt results in a 20-fold increase in melt viscosity. By this increase in melt viscosity, the increase in magma viscosity appears to be explained well (Fig. 5c).

In contrast, the effect of suspended solid particles on viscosity alone does not seem to explain the increase in magma viscosity (Fig. 5c). The magma viscosities obtained in this study are higher than those predicted from the previously investigated model under constant matrix viscosity<sup>29</sup>, i.e., 1.2–5.1 times higher at 1.2–2.7 vol% crystal (Fig. 5c). It has been proposed that the

and the brittle failure of magma with nanocrystals is enhanced by the increment of the relaxation time of the magma.

**Nanocrystal formation controls explosive/non-explosive eruption?** Previous studies<sup>14,33</sup> have proposed that nanocrystal formation in magmas may cause explosive volcanism by enhancing brittle failure of magma. Our experiments demonstrated that nanocrystal formation enhances brittle failure of andesitic magma, and its effect can be explained by the increase in magma viscosity with nanocrystal formation. We also found that the viscosity increase caused by nanocrystal formation in magma is not as large as predicted with analogue materials<sup>14</sup> if the agglomeration of nanocrystals does not take place. Based on these observations, we infer that brittle failure of intermediate composition magmas may not originate from the formation of nanocrystals in actual volcanic eruptions. Here, we estimate the conditions at which brittle failure of magmas with intermediate composition occurs during volcanic eruption and assess whether nanocrystal formation controls the bifurcation between explosive and non-explosive eruptions.

First, the nanocrystal content is limited as long as only magnetite nanocrystals are formed. For instance, the maximum possible crystal contents in the andesite magma used in this study are estimated to be 3–4 vol% based on the total iron content ( $\text{FeO}_t = 6.76 \text{ wt}\%$ ) and the densities of magnetite and andesite melt (5200 and  $2600 \text{ kg m}^{-3}$ ). Therefore, the increment of magma viscosity caused by the formation of magnetite nanocrystals is also not expected to be high, i.e., the maximum increase is within one order of magnitude when our experiments are applied (Fig. 5c). The formation of silicate minerals such as plagioclase and pyroxene can increase the total crystal content and change melt viscosity; however, no experimental studies have confirmed their formation as nanoscale crystals, and additional studies are necessary to clarify the formation of nanoscale silicate minerals. Second, the melt viscosity needed for brittle failure is estimated to be higher than  $10^7 \text{ Pa s}$  when the strain rate yielding in magma is  $< 1 \text{ s}^{-1}$  because the viscosity increases by one order of magnitude during nanocrystal formation. The critical viscosity is  $10^6 \text{ Pa s}$  if we assume a strain rate of  $10 \text{ s}^{-1}$ , corresponding to magma ascent velocity of  $10 \text{ m s}^{-1}$  in a volcanic conduit with a radius of 1 m, and this strain rate seems to be the maximum during magma flow in the conduit with a realistic radius. The local strain rate yielded by bubble expansion would not become larger than the values estimated here, because the pressure in gas bubbles during the growth is almost in equilibrium with melt pressure in low viscosity magma<sup>34</sup>, and the strain rate that is proportional to the difference in the pressure in gas bubbles and in the melt is estimated to be low<sup>35</sup>. Finally, we estimate the condition at which brittle failure of intermediate composition magma can occur. For the andesite magma investigated in this study, the critical viscosity of  $10^6 \text{ Pa s}$  can be achieved at less than  $800 \text{ }^\circ\text{C}$  when the water content is  $> 1 \text{ wt}\%$  and at  $950 \text{ }^\circ\text{C}$  under dry conditions, based on the previous model<sup>23</sup>. In nature, most andesitic magmas have temperatures  $\sim 1000 \text{ }^\circ\text{C}$  and contain a few weight per cent of water<sup>36</sup>. This implies that the formation of only magnetite nanocrystals does not likely lead to brittle failure in andesitic magmas and cannot be the cause of explosive volcanism if the magma temperature does not decrease under dry conditions.

Even if nanocrystal formation in intermediate composition magma does not result in a significant increase in magma viscosity, it may induce explosive eruptions through the rapid heterogeneous formation of gas bubbles<sup>33,37–39</sup>. In particular, magnetite enhances the heterogeneous nucleation of gas bubbles<sup>37,38</sup>. However, the processes of nanocrystal formation during magma ascent remain unclear. In natural and experimental materials including those of

this study, magnetite is a dominant phase as nanocrystal<sup>14,15</sup>. Magnetite stability is strongly influenced by oxygen fugacity, and hence, the redox evolution of magma during ascent may control the formation of nanoscale magnetite, which is determined by volatile degassing<sup>40,41</sup>. If so, the second burst of bubble formation<sup>42,43</sup> that is induced by heterogeneous nucleation on nanoscale magnetite crystals after initial vesiculation and change in redox condition may cause magma fragmentation and hence explosive volcanism.

## Methods

Fibre elongation experiments were performed at BL47XU of SPring-8 (Japan) following the originally developed method<sup>22</sup>. The details of the experimental setup are shown in the Supplementary Information. We first prepared glass fibre with andesitic composition from a volcanic bomb collected at Sakurajima volcano (Japan) in 2003. The powdered rock sample was stored at the laboratory, but the corresponding eruption and sample locality are unclear. The sample can be shared upon request. Sample powder was melted in a Pt crucible at a temperature of  $1500 \text{ }^\circ\text{C}$  for  $> 18 \text{ h}$ ; then, fibrous glass was formed by pulling up a quartz glass attached on the surface of the melt in the Pt crucible<sup>44</sup>. For the glass fibres with lengths of 24–30 mm and diameters of 0.7–0.8 mm, two glass beads of  $\sim 2\text{--}3 \text{ mm}$  in diameter were attached at both ends to hook them on the pistons in the apparatus. The chemical composition of the glass was measured by a scanning electron microscope with a Schottky FE-type gun (JSM-7001F, JEOL Ltd.) and an energy-dispersive X-ray spectrometer (INCA X-act, Oxford Inst.), using the beam scan mode with a beam current of 1.4 nA and a total counting time of 60 s (Supplementary Table 1 and Supplementary Data 1). It was confirmed that the glass fibres contained no crystals, using TEM, SAXS, and WAXD (see the main text). At BL47XU of SPring-8, the fibre was heated to temperatures of 731, 750, 770, 789, 808, and  $828 \text{ }^\circ\text{C}$  using an originally developed furnace, which was mainly made from a boron nitride (BN) cylinder and four cartridge heaters<sup>22</sup>. To prevent a strong signal due to the interaction between the direct X-ray beam and the BN cylinder, a small hole (3 mm in diameter) was set on the side of the BN cylinder. The samples were first heated to the experimental temperature at a rate of  $20\text{--}23 \text{ }^\circ\text{C}$  per minute and then maintained at the experimental temperature for 0, 5, 10, 15, and 30 min. During heating, the sample temperature was homogeneous, because thermal diffusion occurs rapidly, i.e., the diffusion time, defined as  $t = L^2/D$ , where  $L$  and  $D$  are the sample radius ( $< 0.4 \text{ mm}$ ) and thermal diffusivity ( $\sim 0.5 \text{ mm}^2 \text{ s}^{-1}$ )<sup>45</sup>, is estimated to be 0.32 s. Structural relaxation is also expected to be rapid, based on its timescale, i.e.,  $\eta/G$ , where  $\eta$  and  $G$  are the viscosity and shear modulus (10 GPa). In our experiments, the melt viscosity is  $< \sim 10^{10} \text{ Pa s}$ ; thus, the relaxation timescale is  $\sim 1 \text{ s}$ . After heating for 0, 5, 10, 15, and 30 min, the sample was elongated at a constant rate of  $100 \text{ } \mu\text{m s}^{-1}$ . During the experiments, the SAXS, WAXD, and transmit images were obtained every 100 ms. The SAXS and WAXD were measured at 1.8 m and 154 mm from the sample using an original camera and flat panel, respectively. The two-dimensional data obtained were integrated, and the size and volume fraction of the crystals were investigated based on SAXS, while the crystal phase was determined based on WAXD. Sample viscosity was determined based on the load required to deform the sample<sup>46</sup> (see Supplementary Information for details).

## Data availability

All the datasets obtained and discussed in this study are available at <https://doi.org/10.5281/zenodo.7212566>. The data shown in Figs. 2, 4, 5 and Supplementary Fig. 3 are summarised in Supplementary Table 2 and Supplementary Data 1.

Received: 4 January 2022; Accepted: 5 October 2022;

Published online: 17 October 2022

## References

- Papale, P. Strain-induced magma fragmentation in explosive eruptions. *Nature* **397**, 425–428 (1999).
- Zhang, Y. A criterion for the fragmentation of bubbly magma based on brittle failure theory. *Nature* **402**, 648–650 (1999).
- Dingwell, D. B. Volcanic dilemma: flow or blow? *Science* **273**, 1054–1055 (1996).
- Dingwell, D. B. & Webb, S. L. Structural relaxation in silicate melts and non-Newtonian melt rheology in geological processes. *Phys. Chem. Miner.* **16**, 508–516 (1989).
- Rust, A. C., Manga, M. & Cashman, K. V. Determining flow type, shear rate and shear stress in magmas from bubble shapes and orientations. *J. Volcanol. Geotherm. Res.* **122**, 111–132 (2003).
- Okumura, S., Nakamura, M., Nakano, T., Uesugi, K. & Tsuchiyama, A. Shear deformation experiments on vesicular rhyolite: implications for brittle



- fracturing, degassing, and compaction of magmas in volcanic conduits. *J. Geophys. Res.* **115**, B06201 (2010).
7. Wadsworth, F. B. et al. Combined effusive-explosive silicic volcanism straddles the multiphase viscous-to-brittle transition. *Nat. Commun.* **9**, 4696 (2018).
  8. Houghton, B. F. et al. The influence of conduit processes on changes in style of basaltic Plinian eruptions: Tarawera 1886 and Etna 122 BC. *J. Volcanol. Geotherm. Res.* **137**, 1–14 (2004).
  9. Arzilli, F. et al. Magma fragmentation in highly explosive basaltic eruptions induced by rapid crystallization. *Nat. Geosci.* **12**, 1023–1028 (2019).
  10. Picard, D., Arbaret, L., Pichavant, M., Champallier, R. & Launeau, P. The rheological transition in plagioclase-bearing magmas. *J. Geophys. Res.* **118**, 1363–1377 (2013).
  11. Caricchi, L. et al. Non-Newtonian rheology of crystal-bearing magmas and implications for magma ascent dynamics. *Earth Planet. Sci. Lett.* **264**, 402–419 (2007).
  12. Cashman, K. V. Groundmass crystallization of Mount St. Helens dacite, 1980–1986—a tool for interpreting shallow magmatic processes. *Contrib. Mineral. Petrol.* **109**, 431–449 (1992).
  13. Hammer, J. E. & Rutherford, M. J. An experimental study of the kinetics of decompression-induced crystallization in silicic melt. *J. Geophys. Res.* **107**, 2021, <https://doi.org/10.1029/2001JB000281> (2002).
  14. Di Genova, D. et al. In situ observation of nanolite growth in volcanic melt: a driving force for explosive eruptions. *Sci. Adv.* **6**, eabb0413 (2020).
  15. Mujin, M., Nakamura, M. & Miyake, A. Eruption style and crystal size distributions: crystallization of groundmass nanolites in the 2011 Shinmoedake eruption. *Am. Miner.* **102**, 2367–2380 (2017).
  16. Loewen, M. W., Dietterich, H. R., Graham, N. & Izbekov, P. Evolution in eruptive style of the 2018 eruption of Veniaminof volcano, Alaska, reflected in groundmass textures and remote sensing. *Bull. Volcanol.* **83**, 72 (2021).
  17. Lormand, C. et al. Shallow magmatic processes revealed by cryptic microantecrysts: a case study from the Taupo Volcanic Zone. *Contrib. Mineral. Petrol.* **176**, 97 (2021).
  18. Matsumoto, K. & Geshi, N. Shallow crystallization of eruptive magma inferred from volcanic ash microtextures: a case study of the 2018 eruption of Shinmoedake volcano, Japan. *Bull. Volcanol.* **83**, 31 (2021).
  19. Murshed, S. M. S. & Estellé, P. A state of the art review on viscosity of nanofluids. *Renew. Sustain. Energy Rev.* **76**, 1134–1152 (2017).
  20. Liebske, C., Behrens, H., Holtz, F. & Lange, R. A. The influence of pressure and composition on the viscosity of andesitic melts. *Geochim. Cosmochim. Acta* **67**, 473–485 (2003).
  21. Di Genova, D., Zandona, A. & Deubener, J. Unravelling the effect of nano-heterogeneity on the viscosity of silicate melts: implications for glass manufacturing and volcanic eruptions. *J. Non-Cryst. Solids* **545**, 120248 (2020).
  22. Okumura, S. et al. An experimental system for time-resolved x-ray diffraction of deforming silicate melt at high temperature. *Rev. Sci. Instrum.* **91**, 095113 (2020).
  23. Giordano, D., Russell, J. K. & Dingwell, D. B. Viscosity of magmatic liquids: A model. *Earth Planet. Sci. Lett.* **271**, 123–134 (2008).
  24. Duan, X. A model for calculating the viscosity of natural iron-bearing silicate melts over a wide range of temperatures, pressures, oxygen fugacities, and compositions. *Am. Mineral.* **99**, 2378–2388 (2014).
  25. Krieger, I. M. & Dougherty, T. J. A mechanism for non-Newtonian flow in suspensions of rigid spheres. *Trans. Soc. Rheol.* **3**, 137–152 (1959).
  26. Cáceres, F. et al. From melt to crystals: the effects of cooling on Fe–Ti oxide nanolites crystallisation and melt polymerisation at oxidising conditions. *Chem. Geol.* **563**, 120057 (2021).
  27. Cooper, R. F., Fanselow, J. B. & Paker, D. B. The mechanism of oxidation of a basaltic glass: chemical diffusion of network-modifying cations. *Geochim. Cosmochim. Acta* **60**, 3253–3265 (1996).
  28. Magnien, V. et al. Kinetics and mechanisms of iron redox reactions in silicate melts: the effects of temperature and alkali cations. *Geochim. Cosmochim. Acta* **72**, 2157–2168 (2008).
  29. Mader, H. M., Llewellyn, E. W. & Mueller, S. P. The rheology of two-phase magmas: a review and analysis. *J. Volcanol. Geotherm. Res.* **257**, 135–158 (2013).
  30. Prasher, R., Song, D., Wang, J. & Phelan, P. Measurements of nanofluid viscosity and its implications for thermal applications. *Appl. Phys. Lett.* **89**, 133108 (2006).
  31. Rust, A. C. & Cashman, K. V. Multiple origins of obsidian pyroclasts and implications for changes in the dynamics of the 1300 B.P. eruption of Newberry Volcano, USA. *Bull. Volcanol.* **69**, 825–845 (2007).
  32. Wright, H. M. & Weinberg, R. F. Strain localization in vesicular magma: Implications for rheology and fragmentation. *Geology* **37**, 1023–1026 (2009).
  33. Di Genova, D. et al. A compositional tipping point governing the mobilization and eruption style of rhyolitic magma. *Nature* **552**, 235–238 (2017).
  34. Lensky, N. G., Navon, O. & Lyakhovskiy, V. Bubble growth during decompression of magma: experimental and theoretical investigation. *J. Volcanol. Geotherm. Res.* **129**, 7–22 (2004).
  35. Moitra, P., Gonnermann, H. M., Houghton, B. F. & Tiwary, C. S. Fragmentation and Plinian eruption of crystallizing basaltic magma. *Earth Planet. Sci. Lett.* **500**, 97–104 (2018).
  36. Takeuchi, S. Preeruptive magma viscosity: an important measure of magma eruptibility. *J. Geophys. Res.* **116**, B10201 (2011).
  37. Burgisser, A., Arbaret, L., Martel, C., Forien, M. & Colombier, M. The role of oxides in the shallow vesiculation of ascending magmas. *J. Volcanol. Geotherm. Res.* **406**, 107072 (2020).
  38. Cáceres, F. et al. Can nanolites enhance eruption explosivity? *Geology* **48**, 997–1001 (2020).
  39. Hajimirza, S., Gonnermann, H. M. & Gardner, J. E. Reconciling bubble nucleation in explosive eruptions with speedometers. *Nat. Commun.* **12**, 283 (2021).
  40. Burgisser, A. & Scaillet, B. Redox evolution of a degassing magma rising to the surface. *Nature* **445**, 194–197 (2007).
  41. Okumura, S. et al. Decompression experiments for sulfur-bearing hydrous rhyolite magma: redox evolution during magma decompression. *Am. Mineral.* **106**, 216–225 (2021).
  42. Massol, H. & Koyaguchi, T. The effect of magma flow on nucleation of gas bubbles in a volcanic conduit. *J. Volcanol. Geotherm. Res.* **143**, 69–88 (2005).
  43. Kameda, M. et al. Advancement of magma fragmentation by inhomogeneous bubble distribution. *Sci. Rep.* **7**, 16755 (2017).
  44. Goto, A., Taniguchi, M. & Kitakaze, A. Viscosity measurements of hydrous rhyolitic melts using the fiber elongation method. *Bull. Volcanol.* **67**, 590–596 (2005).
  45. Hofmeister, A. M., Whittington, A. G. & Pertermann, M. Transport properties of high albite crystals, near-endmember feldspar and pyroxene glasses, and their melts to high temperature. *Contrib. Mineral. Petrol.* **158**, 381–400 (2009).
  46. Taniguchi, M. Entropy dependence of viscosity and the glass-transition temperature of melts in the system diopside-anorthite. *Contrib. Mineral. Petrol.* **109**, 295–303 (1992).

## Acknowledgements

We thank three reviewers for their critical reviews. This study received financial support from Grants-in-aid for Scientific Research in Japan (Nos. 18H01296, 19K21889, 19H00721 and 22H00161).

## Author contributions

S.O. designed the research plan and wrote the manuscript. S.O., K.U., and A.T. developed an experimental system and S.O., A.G., T.S., and K.M. performed experiments at SPring-8. A.G. prepared glass fibres for elongation experiments. A.M. performed TEM analyses.

## Competing interests

The authors declare no competing interests.

## Additional information

**Supplementary information** The online version contains supplementary material available at <https://doi.org/10.1038/s43247-022-00573-9>.

**Correspondence** and requests for materials should be addressed to Satoshi Okumura.

**Peer review information** Communications Earth & Environment thanks Danilo Di Genova, Francisco Cáceres and the other, anonymous, reviewer(s) for their contribution to the peer review of this work. Primary Handling Editors: Emma Liu, Joe Aslin.

**Reprints and permission information** is available at <http://www.nature.com/reprints>

**Publisher's note** Springer Nature remains neutral with regard to jurisdictional claims in published maps and institutional affiliations.



**Open Access** This article is licensed under a Creative Commons Attribution 4.0 International License, which permits use, sharing, adaptation, distribution and reproduction in any medium or format, as long as you give appropriate credit to the original author(s) and the source, provide a link to the Creative Commons license, and indicate if changes were made. The images or other third party material in this article are included in the article's Creative Commons license, unless indicated otherwise in a credit line to the material. If material is not included in the article's Creative Commons license and your intended use is not permitted by statutory regulation or exceeds the permitted use, you will need to obtain permission directly from the copyright holder. To view a copy of this license, visit <http://creativecommons.org/licenses/by/4.0/>.

© The Author(s) 2022